International Journal of Applied Earth Observation and Geoinformation 38 (2015) 280–291

Contents lists available at ScienceDirect

International Journal of Applied Earth Observation and Geoinformation

journal homepage: www.elsevier.com/locate/jag

Integration of WorldView-2 and airborne LiDAR data for tree species level carbon stock mapping in Kayar Khola watershed, Nepal

Yogendra K. Karna[a,1], Yousif Ali Hussin[b,2], Hammad Gilani[c,d,*], M.C. Bronsveld[b,2], M.S.R. Murthy[c], Faisal Mueen Qamer[c], Bhaskar Singh Karky[c], Thakur Bhattarai[e], Xu Aigong[d], Chitra Bahadur Baniya[f,3]

[a] Department of Forests, Ministry of Forests and Soil Conservation, Babarmahal, Kathmandu, Nepal
[b] Department of Natural Resources, Faculty of Geo-information Science and Earth Observation (ITC), University of Twente, 7500 AE Enschede, The Netherlands
[c] International Centre for Integrated Mountain Development (ICIMOD), GPO Box 3226, Khumaltar, Lalitpur, Nepal
[d] School of Geomatics, Liaoning Technical University, 47 Zhonghua Road, Fuxin, Liaoning Province, China
[e] Centre for Environmental Management Central Queensland University, Rockampton Queensland 4702, Australia
[f] Central Department of Botany, Tribhuvan University, Kirtipur, Nepal

ARTICLE INFO

Article history:
Received 19 June 2014
Received in revised form 16 January 2015
Accepted 22 January 2015

Keywords:
Airborne LiDAR
CHM
CPA
Image classification
Multi-resolution segmentation
WorldView-2

ABSTRACT

Integration of WorldView-2 satellite image with small footprint airborne LiDAR data for estimation of tree carbon at species level has been investigated in tropical forests of Nepal. This research aims to quantify and map carbon stock for dominant tree species in Chitwan district of central Nepal. Object based image analysis and supervised nearest neighbor classification methods were deployed for tree canopy retrieval and species level classification respectively. Initially, six dominant tree species (*Shorea robusta, Schima wallichii, Lagerstroemia parviflora, Terminalia tomentosa, Mallotus philippinensis and Semecarpus anacardium*) were able to be identified and mapped through image classification. The result showed a 76% accuracy of segmentation and 1970.99 as best average separability. Tree canopy height model (CHM) was extracted based on LiDAR's first and last return from an entire study area. On average, a significant correlation coefficient (r) between canopy projection area (CPA) and carbon; height and carbon; and CPA and height were obtained as 0.73, 0.76 and 0.63, respectively for correctly detected trees. Carbon stock model validation results showed regression models being able to explain up to 94%, 78%, 76%, 84% and 78% of variations in carbon estimation for the following tree species: *S. robusta, L. parviflora, T. tomentosa, S. wallichii* and others (combination of rest tree species).

Introduction

A number of different methods are currently being used to measure aboveground biomass (AGB) and consequently, the stock of forests. Lu (2006) reviewed and summarized some of these approaches to estimate forest biomass based on field measurements, remote sensing (RS) and geographic information systems (GIS). RS approaches provide an alternative to traditional methods which give spatially explicit information and enable repeated monitoring, even in remote locations, in a cost-effective way (Patenaude et al., 2005). With its capacity to provide spatial, temporal and spectral information, RS can estimate sequestered carbon more accurately and thus meet the requirements of the Kyoto Protocol and the United Nations collaborative programme on reducing emissions from deforestation and forest degradation (REDD) (Gibbs et al., 2007; Joseph et al., 2013).

Optical remote sensing measurements have been widely used in studies that link AGB measurements from the field to satellite observations, based on sensitivity of the optical reflectance to variations in canopy structure. (Song and Dickinson, 2008). Medium spatial resolution data, such as Landsat TM, provides the potential for AGB estimation at a national and regional level, but the mixed

* Corresponding author at: International Centre for Integrated Mountain Development (ICIMOD), GPO Box 3226, Khumaltar, Lalitpur, Nepal. Tel.: +977 1500322.
E-mail addresses: y.karna@dof.gov.np (Y.K. Karna), y.a.hussin@utwente.nl (Y.A. Hussin), Hammad.Gilani@icimod.org (H. Gilani), bronsveld@itc.nl (M.C. Bronsveld), Manchiraju.Murthy@icimod.org (M.S.R. Murthy), Faisal.Qamer@icimod.org (F.M. Qamer), Bhaskar.Karky@icimod.org (B.S. Karky), t.bhattarai@cqu.edu.au (T. Bhattarai), xu_ag@126.com (X. Aigong), cb.baniya@cdbtu.edu.np (C.B. Baniya).
[1] Tel.: +977 9841781224.
[2] Tel.: +31 534874293.
[3] Tel.: +977 9849421945.

http://dx.doi.org/10.1016/j.jag.2015.01.011
0303-2434/

pixels, cloudy weather and data saturation are found to be problems in complex biophysical environments (Lu, 2005). Although RADAR backscatter can penetrate through clouds, it poses a saturation problem in tropical forest environments where AGB levels generally exceed 200–250 Mg/ha (Ustin, 2004). Sometimes mountainous and hilly conditions further increase the errors (Thapa et al., 2014b; Toan et al., 2004). To overcome this problem, active optical RS sensors, e.g., airborne laser scanning or airborne LiDAR, offer promising mapping techniques to estimate forest biomass as no saturation is observed at high biomass levels (Patenaude et al., 2005; Huang et al., 2013). Lefsky et al. (2002) and Lim et al. (2003) both reviewed the potential of LiDAR devices for retrieving forest parameters. LiDAR data was used to estimate the biomass of the Douglas fir western hemlock (Means et al., 1999), temperate mixed deciduous forest biomass (Ahmed et al., 2013; Peduzzi et al., 2012), tropical forest biomass (Asner et al., 2012; Kronseder et al., 2012), tree height and stand volume (Yamamoto et al., 2010), stand height (Wulder and Seemann, 2003), tree crown diameter (Kwak et al., 2007; Popescu et al., 2003) and canopy structure (Lovell et al., 2003). Other researches tend to indicate that either the use of LiDAR data alone, or its use in combination with other sensor or ancillary data, provides an important data source for forest parameters estimation (Drake et al., 2003; Hyde et al., 2006). Holmgren et al. (2008) presented the benefits of integrating Quickbird multispectral imagery and high-density LiDAR data for individual tree-based classification, increasing the accuracy of observation from 88 to 96%. Similarly, Leckie et al. (2003) fused high-density LiDAR data and digital camera imagery for suitable tree crown isolation and tree height measurement; the results showed 80–90% correspondence with ground reference tree delineation. Crown diameter or crown projection area (CPA) can be obtained from very high resolution (VHR) satellite imagery, whereas tree height can be easily obtained from the canopy height model developed from LiDAR data. Several studies (Breidenbach et al., 2010; Gautam et al., 2010; Huang et al., 2009; Jochem et al., 2011; Katoh et al., 2009; Kim et al., 2010; Lindberg et al., 2008; Lu, 2006; Thapa et al., 2014a) also showed that the integration of VHR satellite images and airborne LiDAR data provide an accurate and efficient measurement of AGB in a variety of forest types and in extensively larger areas.

Nepal falls under the category of data-scarce countries, especially in terms of derived remotely sensed data products. This study was conducted in one of the REDD+ pilot project site where community forestry programme was introduced 30 years ago to reduce deforestation and forest degradation (ICIMOD, 2012). The objective of this paper is to develop an approach for a more accurate estimation of carbon stock for broadleaved tree species predominantly found in Nepal's tropical forests, testing the use of WorldView-2, airborne LiDAR and field data. In this paper, image segmentation technique was adopted for delineation of individual tree crowns from VHR WorldView-2 image. Similarly, LiDAR based canopy height model (CHM) was statistically evaluated through field-based tree height information.

Materials and methods

Study area

Kayar Khola watershed in the north-eastern part of Chitwan district, Nepal, covers an area of 800 ha and encompasses plains and small Siwalik Hills in its territory. Altitude in the watershed ranges from 235 to 1935 above mean sea level (amsl). The average maximum and minimum temperature of the district is 30 and 16 degrees Celsius, respectively. The average annual rainfall of the district is 1510 mm/year. Of the total area, 5821 ha is covered by forests, of which 2384 ha are community forests (CFs) managed by at least 16 community forests user groups (CFUGs). Out of sixteen organized CFUGs in the study area, only seven CFs from three different village clusters, covering an area of 871 ha, were selected for this research, representing diverse types of forest structures (Fig. 1). Site selection is based on area accessibility in terms of steepness, road distance from Kathmandu (the capital city), data availability, variation in terrain, and prior implementation of REDD+ pilot project.

Mixed forests exist within the watershed, with *Shorea robusta* (Sal) being the most dominant species, mostly found in the southern aspects and in lower altitudes of the northern aspects of the watershed. *Schima wallichii* (Chilaune), followed by a few other associated species, such as *Lagerstroemia parviflora* (Botdhairo), *Adina cordifolia* (Haldu), *Terminalia tomentosa* (Asna), *Syzizium cumini* (Jamun), *Ficus racemosa* (Dumri), *Terminalia bellirica* (Barro), *Rhus wallichii* (Kag Bhalayo), *Bombax ceiba* (Simal), *Garuga pinnata* (Dabdabe), and *Albizia* species thrive in the area.

Data and software used

The number of sample units were calculated using Eq. (1) developed by Husch et al. (2003). From 22 September to 20 October 2011, a total of 75 plots were measured in seven CFs of the watershed, although it was intended through formula to measure only 72 plots. On each 500 m^2 circular plot, the DBH, height, and species of existing trees were recorded. Ordinary global positioning system (GPS) receiver for location identification, TruPulse 360 B for tree height measurement and diameter tape for DBH measurement, were used in the field. DBH, height and crown diameter of each major dominant tree species was analysed and presented in box-whisker plot to identify outliners and to further process the data.

$$N_{\text{plots}} = t^2 \times \text{CV}^2 \left(\frac{1}{E}\right)^2 \quad (1)$$

where N_{plots} is the minimum number of sample plots, t^2 is the value of the student's distribution for N_{plots} at desired probability, CV^2 is coefficient of variation (%) of diameter at breast height (DBH) of trees to be sampled and E is the estimated allowable error or desired precision (%) for DBH of trees sampled. Twenty per cent (20%) is the common starting point for E (Husch et al., 2003).

The study used ortho-rectified WorldView-2 first commercial 8 bands VHR satellite imagery obtained on 25 October 2010. It has a VHR spectral coverage that includes two bands of blue (blue and coastal blue), followed by green, yellow, red, rededge and two bands of near infrared (NIR1 and NIR2). The imagery has 2 m multispectral and 0.5 m panchromatic spatial resolution. The NIR1 band has the potential to identify vegetation type at species level (Pu and Landry, 2012).

Airborne LiDAR data was acquired between 16 March and 2 April 2011 using Leica ALS-40 sensor positioned on a helicopter at 2000 m flying altitude, with average point density of 0.8 /m^2 at the ground level and sensor scan speed of 20.4 lines/s. LiDAR data was acquired at average horizontal and vertical accuracies of 0.45 m each.

Image processing was done in ERDAS Imagine, LiDAR in LASTools, Quick Terrain Modeller and ArcMap used for mapping and XLStat, SPSS and R studio for statistical analysis. Image segmentations were done in eCognition Developer. The methodological flow diagram for this research is shown in Fig. 2.

Pre-processing of remotely sensed data

For this study, ortho-rectified WorldView-2 multispectral images of 2 m resolution and panchromatic imagery of 0.5 m resolution were fused to get a pan-sharpened image of 0.5 m spatial resolution using hyperspherical color sharpening (HCS)

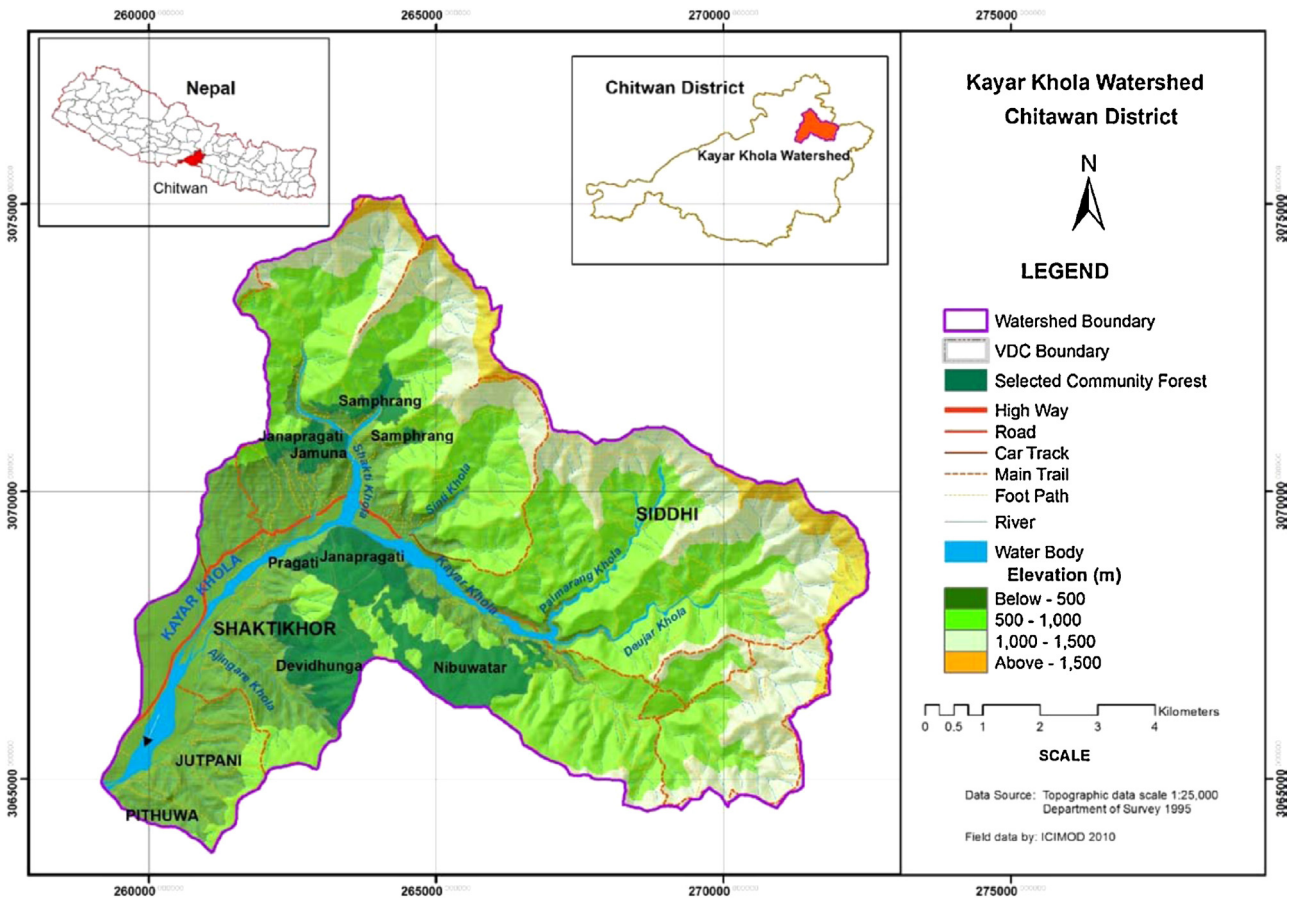

Fig. 1. Location map of study area.

technique, applying bilinear interpolation resampling technique, smoothening filter size 5 and unsigned 16 bit output data type. Padwick et al. (2010) found that HCS algorithm maintains the best balance between spectral and spatial quality imagery when compared among four algorithms, i.e., HCS, hue intensity saturation (HIS), principal components analysis (PCA) and gramm schmidt (GS).

For VHR satellite image and LiDAR point cloud data, registration was necessary because of differences in time acquisition and perspectives, or even sensors (Toth et al., 2011). LiDAR data turned out to be more accurate than satellite image as it has *x*, *y* and *z* coordinates of each point on the ground and is already geo-referenced to WGS 1984 UTM Zone 45N. Each coordinate was collected through GPS receiver installed in a helicopter with an inertial measurement unit (IMU).

Although WorldView-2 data was sensor-based rectified (Ortho Ready Standard-2A), positional error was still observed in the data through collected GPS coordinates and visual image interpretation. Altogether, 26 points were taken as ground control points (GCPs) on WorldView-2 by considering LiDAR data as a reference, resulting in an overall root mean square error (RMSE) of 1.2 m for panchromatic and 1.5 m for multispectral image.

The study used 5 returns airborne LiDAR point cloud. Only the first and last returns were used while the remaining three return points represented the stroked back values from the tree trunks, branches and leaves. First-return points were interpolated to a regular grid that corresponds to the digital surface model (DSM), whereas the last return points were interpolated as digital terrain models (DTMs). Each of the extracted DSM and DTM pixel size was 0.5 m. DTM was subtracted from DSM to obtain CHM (0.5 m). Tree height collected from the field and CHM derived from LiDAR data were evaluated using Pearson's correlation coefficient and one-way ANOVA.

CPA delineation and validation

Many researchers have been studying individual tree crown delineation or segmentation using VHR satellite images (Erikson and Olofsson, 2005; Ke and Quackenbush, 2011a,b; Koch et al., 2006; Pu and Landry, 2012). For this research, multi-resolution segmentation technique was applied to segment tree crown onto fused LiDAR and WorldView-2 data. This method identified geographical features using scale and homogeneity parameters obtained from the spectral reflectance values in different bands from WorldView-2 image and elevation values in the CHM. Out of eight spectral bands of pan-sharpened imagery, only three bands (NIR1, NIR2 and Red-Edge) and a CHM layer were given higher weight for segmentation for spectral separability of tree species and thus, regarded as important for tree crown delineation. For the selection of best-fit scale parameters, the estimation of scale parameter tool (Lobianco and Esposti, 2010) was used in the segmentation procedure. The segmentation process was done using 21 as scale parameter, 0.8 as shape and 0.6 as compactness value. Morphological operation was applied to reshape the advanced object of image.

From the field, a total of 1147 trees were measured, but only one-third could be easily recognized in the image for manual digitization or delineation. The delineation of recognized tree crowns were used for assessment segmentation accuracy and model validation. Accuracy assessment of tree crown segmentation was done using the method proposed by Möller et al. (2007) and Clinton et al. (2010). Möller et al. (2007) developed an accuracy assessment method based on visual techniques, also known as relative

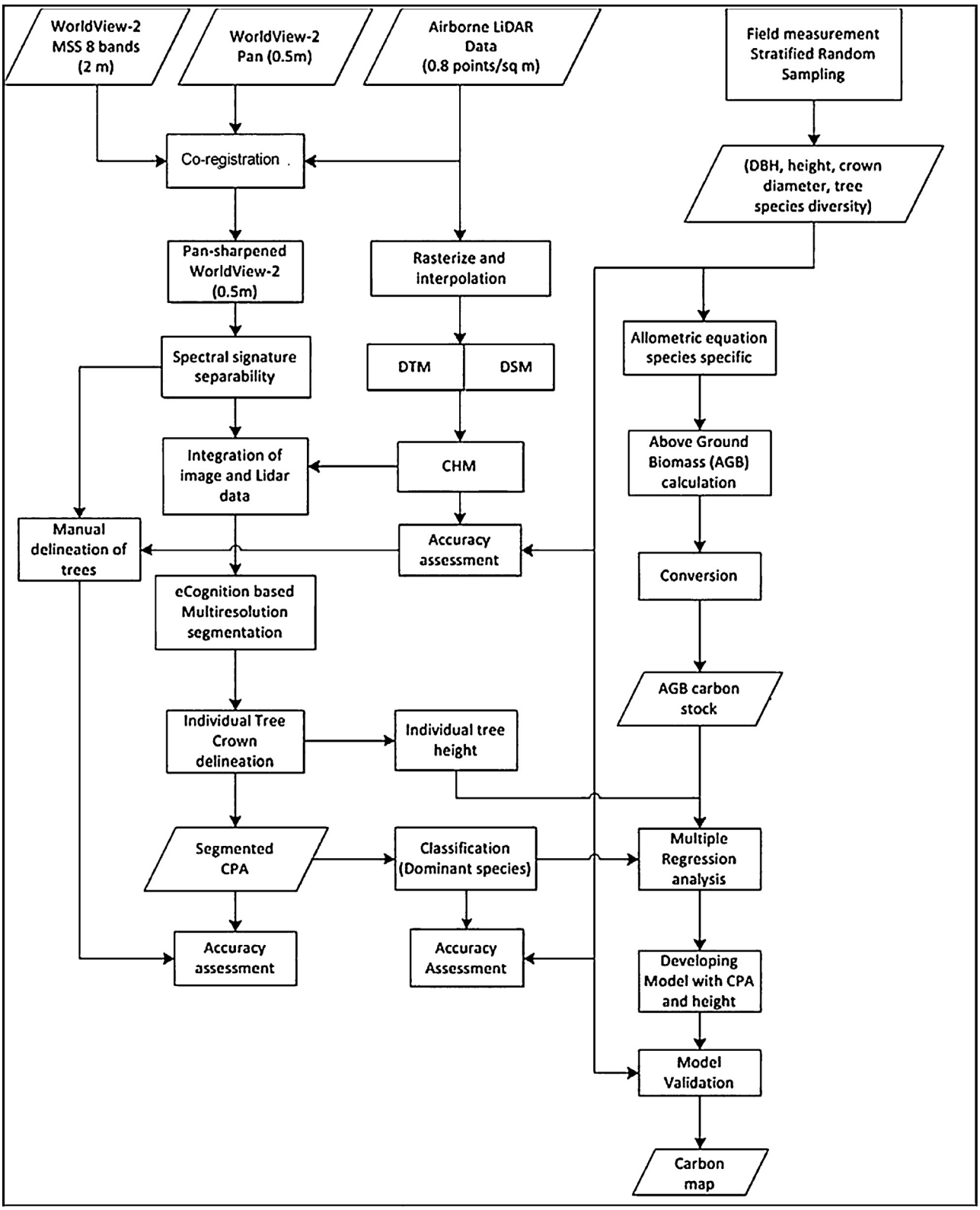

Fig. 2. Methodology flow diagram.

area approach, to validate the segmentation using reference delineated from a manual. Clinton et al. (2010), on the other hand, developed a geometrical segmentation accuracy assessment of segmented outputs with reference to clearly defined training sets. The quality of segmentation outputs are defined in terms of over and under segmentation (Eqs. (2) and (3)), as well as closeness of fit (Eq. (4)). *D* value is interpreted as the 'closeness' measure to an ideal segmentation result in relation to a pre-defined reference set and ranges from 0 to 1. As the value of *D* increases, the deviation of segmented objects and their respective refer-

Table 1
Model parameters for biomass estimation and wood density of major tree species.

Species	*a*	*b*	*c*	R^2	Wood density (kg/m^3)
S. robusta	−2.4554	1.9026	0.8352	98.3	880
S. wallichii	−2.7385	1.8155	1.0072	98.3	689
L. parviflora	−2.3411	1.7246	0.9702	97.5	850
Adina cordifolia	−2.5626	1.8598	0.8783	98.1	670
T. tomentosa	−2.4616	1.8497	0.8800	98.9	950
Albizia species	−2.4284	1.7609	0.9662	97.8	673
S. cumini	−2.5693	1.8816	0.8498	98.3	770
Miscellaneous species in Terai	−2.3993	1.7836	0.9546	98.3	720

ence object increases, indicating a high level of mismatch between objects.

$$\text{Over segmentation}_{ij} = 1 - \frac{\text{area}(x_i \text{n} y_j)}{\text{area}(x_i)} \quad (2)$$

$$\text{Under segmentation}_{\text{ij}} = 1 - \frac{\text{area}(x_i \text{n} y_j)}{\text{area}(x_i)} \quad (3)$$

where x_{i} is the training objects or reference relative to which the segmentation will be judged and y_{j} is the set of all segments in the segmentation.

$$D = \sqrt{\frac{\text{Over segmentation}_{ij}^2 + \text{Under segmentation}_{ij}^2}{2}} \quad (4)$$

Tree species classification and accuracy assessment

In this study, supervised nearest neighbor classification was applied to classify tree crowns at species level. To generate smart objects with multi-resolution segmentation and supervised classification, nearest neighbor classification is a powerful approach (Belgiu and Drăguţ, 2014). The mean value of NIR1, NIR2 and red-edge band of pan-sharpened image and the maximum value of CHM were chosen in object features for classification. The image objects (tree crown) were classified into six tree species on the basis of training data collected from the field. The tree that was clearly recognized and annotated in both image and in the field was used as training sample for classification. Seventy percent (70%) of sample trees recognized in the image were used as training samples, while the remaining 30% were used as test data for accuracy assessment in the case of each major dominant tree species.

Allometric equation and carbon stock estimation

In the absence of species-specific biomass equation of trees in this study, species-specific volume equations developed by Sharma and Pukkala (1990) were used to estimate AGB of forests (Eq. (5)). The estimated parameter values of *a*, *b* and *c* for different species and wood densities of the major tree species are given in Table 1. The obtained volume was multiplied with dry wood density (specific gravity) of the species to get air dry weight of stem biomass (Chaturvedi and Khanna, 1982) using Eq. (6). The biomasses of branches and leaves (foliage) were estimated to be 42% and 8% of the stem biomass, respectively (Sharma, 2011) to calculate total biomass of trees (Eq. (7)). The total AGB thus obtained total carbon stock of individual trees, using a conversion factor of 0.47 (Eq. (8)) as suggested by IPCC (2006).

$$\ln(V) = a + b \times \ln(\text{DBH}) + c \times \ln(\text{Ht}) \quad (5)$$

where 'ln' is natural logarithm, *V* is the total stem volume with bark in m^3, to obtain the volume in cubic meters. The prediction is to be divided by 1000, where DBH is the diameter at breast height (in cm), Ht is the tree height in meters and *a*, *b* and *c* are contact model parameters.

$$\text{Stem biomass} = \text{Stem volume} + \text{Wood densit} \quad (6)$$

$$\text{Total AGB=Stem biomass+Branch biomass+Foliage biomass} \quad (7)$$

$$\text{Total Carbon Stock} = \text{Total AGB} \times 0.47 \quad (8)$$

Statistical analysis

A scatter diagram of two related variables was depicted in order to see the relationship between these variables; the relationship, for example, between field-measured CPA and image CPA, field height and LiDAR-derived height, carbon and CPA and carbon and LiDAR-derived height. Correlation coefficients (*r*) and coefficient of determination (R^2) were calculated, which showed the percentage of variation in one variable associated to other variables and can be explained by the given regression (Yaroshenko et al., 2001). Multiple linear regression analysis was employed using field-measured carbon stock as the response variable and CPA and LiDAR-derived height as explanatory variables. In order to avoid multi-collinearity amongst explanatory variables (i.e., CPA and height), a tolerance limit less than 10 of the variance inflation factor, VIF = $1/(1 - R_{\text{i}}^2)$ was used, where R_{i}^2 is the multiple correlation of the variable with all other explanatory variables in the regression model.

The classified individual tree that has a one to one spatial correspondence with reference and delineated tree crowns were used for model development and validation, since misclassified trees cannot be used for evaluation (Flewelling et al., 2008; Pouliot et al., 2002). The model obtained was validated with 30% of field-measured data in the case of each major dominant tree species. R^2 and root mean square error (RMSE) were used to assess performance of the model. RMSE explains the difference between model-predicted values and calculated values. RMSE in percentage was calculated from the ratio of RMSE and average calculated carbon (Eq. (9)). The carbon stock for the entire study area was calculated for each CF and species using the validated regression model (Eq. (10)).

$$\text{RMSE} = \sqrt{\sum_{i=1}^{n} \frac{(\text{Y}j - \hat{\text{Y}}j)^2}{n}} \quad (9)$$

where Y_i is the measured/calculated value of carbon, $\hat{Y}_i$ is the predicted carbon value by the model and *n* is the number of samples.

$$\ln\text{Carbon} = \beta 0 + \beta 1 \times \ln(\text{CPA}) + \beta 2 \times \ln(\text{Height}) \quad (10)$$

where 'ln' is natural logarithm, carbon is aboveground carbon stock per tree in kg, β0 is intercept, β1 is coefficient of CPA, β2 is coefficient of LiDAR-derived tree height.

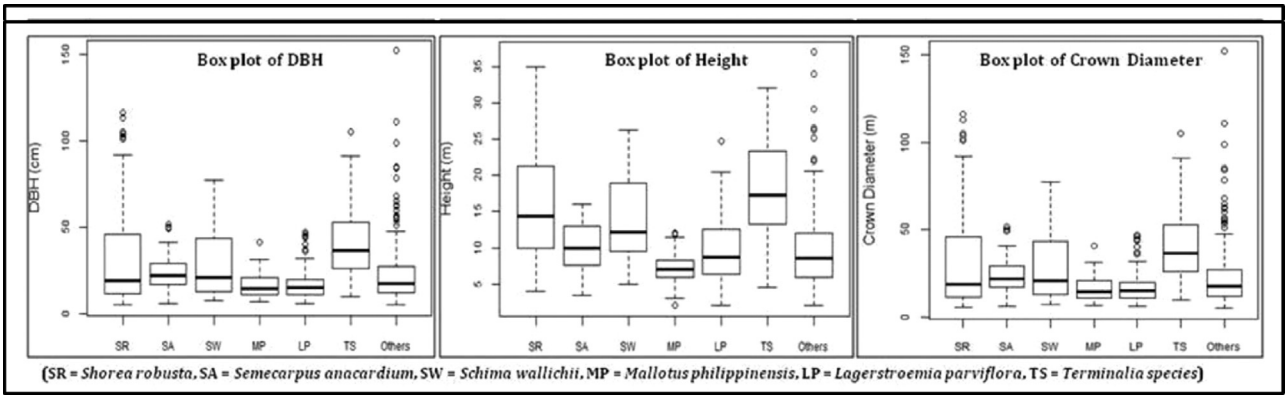

Fig. 3. Box plot of DBH, height and crown diameter of major tree species.

Results

Descriptive analysis of field data

Forest stand parameters (DBH, height and crown diameter) were measured for each sampled tree in every sampling plot for all seven CFs covered by the study. In total, the DBH of 1147 trees and the height and crown diameters of 727 and 497 trees in 75 plots were measured. Forest inventory revealed 72 species growing in the study area, although there are only six dominant species. Some 73% of the watershed's forests was dominated by these six species, with *S. robusta* as the most predominant (42%), followed by *L. parviflora* (12%) and three other major species covering 5% each of forest cover. *Semecarpus anacardium* contributes 4% of species composition. Four other major identified tree species have an 8% contribution, while the rest of the species generally categorized as 'miscellaneous' contributed 19% of forest cover.

On average, species in the 'others' category had the largest DBH and was the tallest, followed by *S. robusta* and *Terminalia* species, whereas *Terminalia* species had the largest crown diameter, followed by *S. robusta*, *S. wallichii* and others. Moreover, these species have the highest variability in terms of DBH and height as well as crown diameter (Fig. 3).

Validation of segmention CPA

Validation of tree crown segmentation was obtained using accuracy measures of D and 1:1 spatial correspondence for 344 manually-delineated referenced tree crowns. Over-and under-segmentation and D were 0.29, 0.34 and 0.33, respectively. Total accuracy of tree crowns delineation was about 67%, which means a segmentation error of 33%. *D* value was lowest at 0.29 in Jamuna CF, implying a lower over-segmentation error, whereas Janpragati and Pragati CFs yielded higher *D* values of 0.40 and 0.39, respectively. A one to one spatial correspondence matching of referenced and segmented crowns was observed in the study areas. Out of 344 reference polygons obtained from manual delineation, only 261 automatic polygons were obtained from segmentation and overall, a 76% accuracy of segmentation was achieved (Table 2).

Validation of height and CPA

A total of 205 tree heights measured in the field and corresponding LiDAR heights extracted from manual delineation of tree crown were used as sample datasets. R^2 and adjusted R square showed that LiDAR derived height was best predicted at 76% with 3.84 m RMSE (Fig. 4). Based on Pearson's Correlation test and one-way analysis of variance (ANOVA) test, there was no significant difference between heights measured from the field and those derived from LiDAR data (Table 3).

Tree species classification and accuracy assessment

To assess the potential of WorldView-2 eight spectral bands to differentiate tree species, transformed divergence was calculated on the basis of field training dataset for different major tree species, as shown in Table 4. Separability can be evaluated for any combination of bands that is used in the classification, enabling you to rule out any bands that are not useful in the results of the classification. The best average separability was 1970.99, which indicates an image with a good separation among several species. Excellent separability between *S. anacardium* and *Mallotus philippinensis, S. wallichii* and *T. tomentosa*, *M. philippinensis* and *S. wallichii, and S. anacardium* and *T. tomentosa* was found with D_T of 2000. *S. robusta* and *L. parviflora* had the best separability, with separability among the rest of the species shown in Table 4, because it had values all greater than 1900.

All seven CFs were segmented in four clusters, because many species were identified, mostly not common to all CF areas of the study, resulting in large datasets that could not all be processed in one run. The CF clusters included: (1) Devidhunga, (2) Nibuwatar, (3) Janpragati B and (4) Samphrang, Jamuna, Janpragati and Pragati (Fig. 5). Of the CF clusters, cluster (1) Janpragati B CF had the highest overall accuracy rates and Kappa statistics for three species,

Table 2
Matching 1:1 correspondence of reference polygons to segmented polygons of CPA.

Community forest area	Number of reference polygons	1:1 correspondence	Correctly segmented CPA (%)
Devidhunga	97	75	77.32
Nibuwatar	102	73	71.57
Janpragati B	32	25	78.13
Samphrang	47	39	82.98
Janpragati	13	9	69.23
Jamuna	18	12	66.67
Pragati	35	28	80.00
Overall accuracy	344	261	75.87%

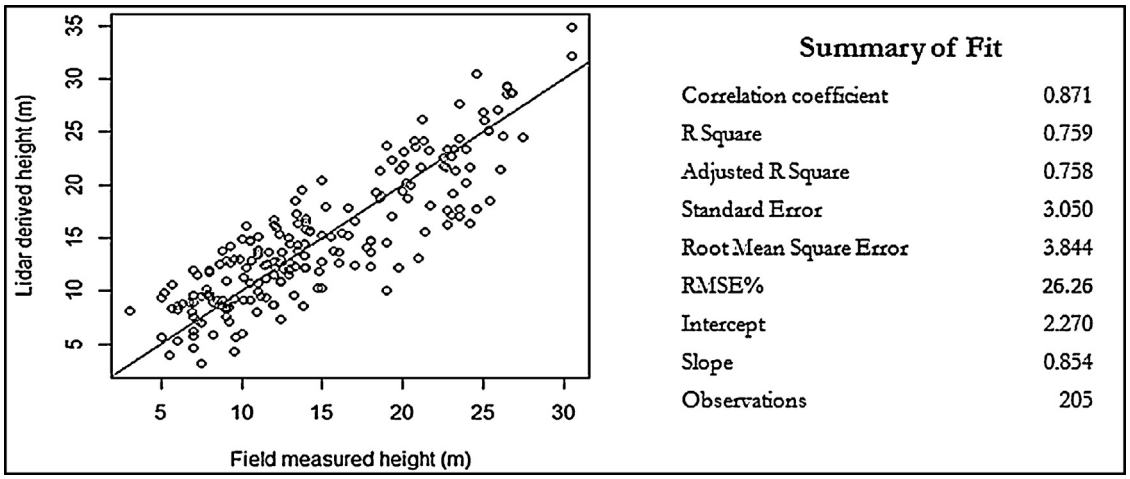

Fig. 4. Summary of tree height from field and LiDAR.

Table 3
Summary of statistical tests – Tree heights from field and LiDAR.

Test	df	Test stat	*P* value	Test critical
Pearson's correlation	203	0.871	0.527	0.178
One way ANOVA	1408	0.051	0.820	3.864
Conclusion: *r* statistic is greater than critical value of *r* so null hypothesis is rejected i.e., there is a statistically significant relationship between height measured from the field and that derived from LiDAR ($P < 0.05$)				
Conclusion: *F* statistic is less than *F* critical so the two means are not statistically significantly different, i.e., there is no significant difference between height measured from the field and derived from LiDAR ($P < 0.05$)				

Table 4
Transformed divergence between pairs of tree species using WorldView-2 image and measure of average separability.

Tree species	*L. parviflora*	*T. tomentosa*	*S. robusta*	*S. wallichii*	*M. philippinensis*	*S. anacardium*
S. robusta	1911.81	1908.29	0	1984.51	1933.01	1996.34
S. wallichii	1998.25	2000	1984.51	0	2000	1982.64
L. parviflora	0	1907.41	1911.88	1998.25	1947.53	1996.7
T. tomentosa	1907.41	0	1908.29	2000	1999.14	2000
M. philippinensis	1947.53	1999.14	1933.01	2000	0	2000
S. anacardium	1996.7	2000	1996.34	1982.64	2000	0
Best average separability:1970.99						

while the Nibuwatar CF was the lowest-ranked cluster based on overall accuracy and Kappa statistics, with five identified and classified species. Eighteen of 31 reference tree crowns at Devidhunga CF were correctly classified, with an overall accuracy rate of 58.06% and Kappa statistics of 0.47; six species were classified in the area. Four CF clusters had moderate overall accuracy rates of 62.50% and Kappa statistics of 0.48, with five identified and classified tree species in these clusters*: S. robusta, L. parviflora, M. philippinensis* and *S. anacardium*. There was 100% user's accuracy in the case of Janpragati B, Nibuwatar and Devidhunga CFs. The tree species *T. tomentosa* achieved 100% user's accuracy in the case of Devidhunga CF and four other CFs. *S. wallichi* and other classes had lower user's accuracy rates compared to the rest of the tree classes for all CF areas. *Shorea robusta* was classified in all four clusters of CF areas, with more than 65% user's accuracy (Table 5).

Carbon stock mapping

Based on gathered and analysed data, the amount of carbon per tree varied from less than 500 kg/tree to more than 2000 kg/tree. A few big trees with large CPA and height had more than 5000 kg carbon stock, with a good indication reported for *S. robusta* and *T. tomentosa*, *L. parviflora*, *S. wallichii* and most of the species from the 'others' or 'miscellaneous' category had less carbon stock ranging

Table 5
User's and producer's accuracy of species classification.

	Devidhunga		Nibuwatar		Janpragati B		Samphrang, Jamuna, Janpragati and Pragati	
Tree species	User accuracy	Producer accuracy	User accuracy	Producer accuracy	User accuracy	Producer accuracy	User accuracy	Producer accuracy
S. robusta	66.67	85.71	75	50	100	60	71.43	62.5
S. wallichii	–	–	50	100	66.67	100	–	–
L. parviflora	75	75	100	50	–	–	50	50
T. tomentosa	100	25	42.86	50	–	–	100	75
M. philippinensis	100	66.67	–	–	–	–	66.67	40
S. anacardium	100	50	–	–	–	–	–	–
Others	35.71	62.5	33.33	50	50	66.67	56.25	66.67

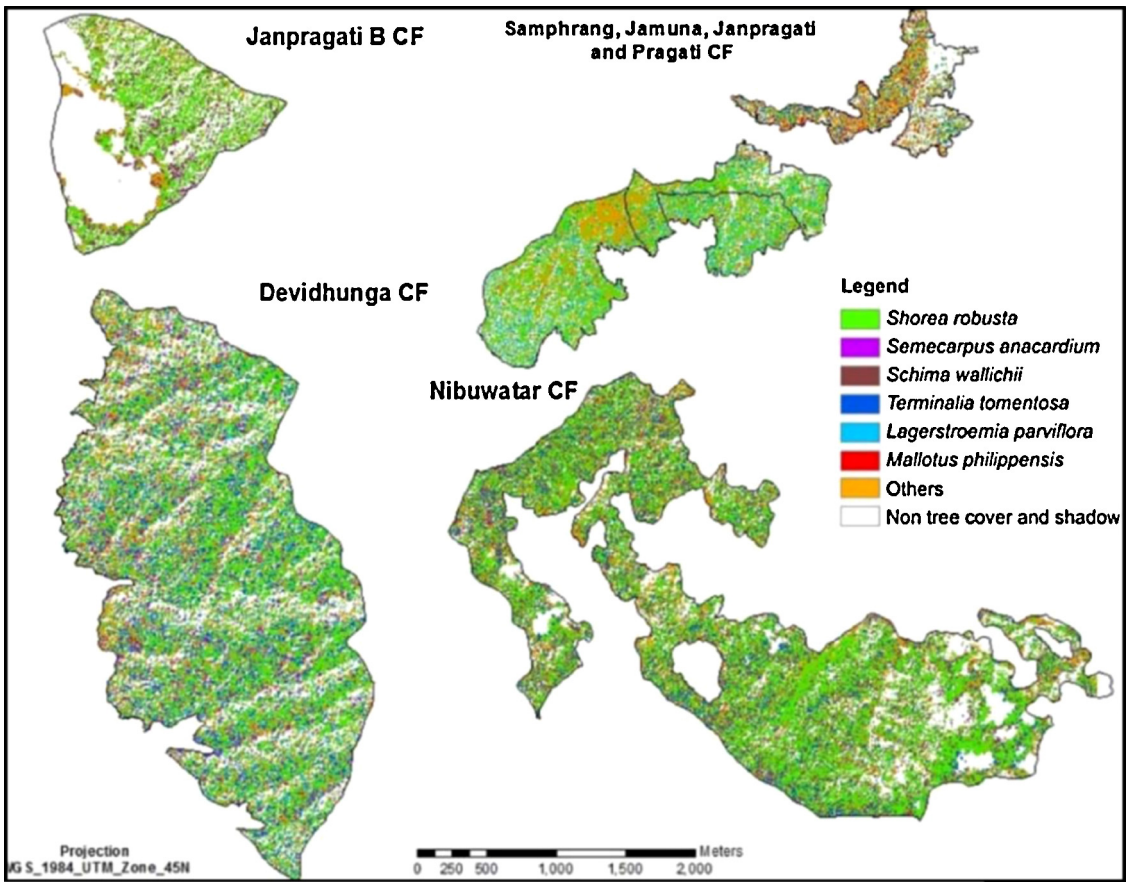

Fig. 5. Tree species classification map of study area.

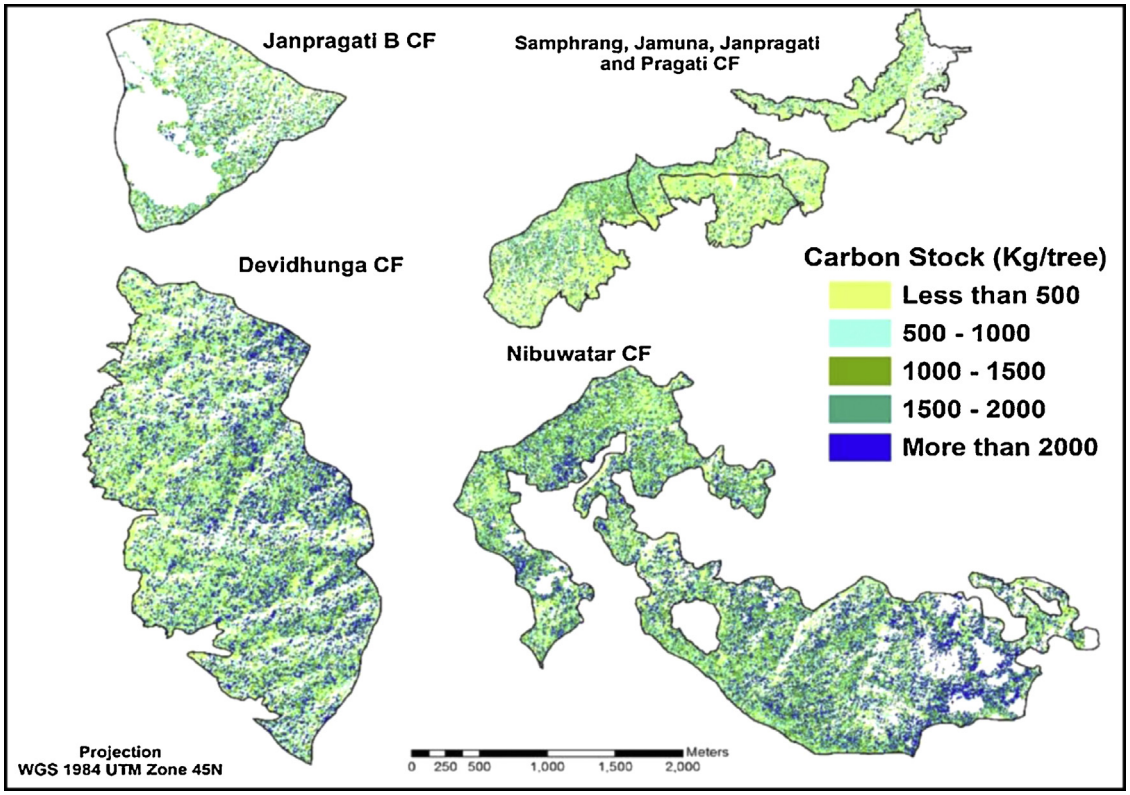

Fig. 6. Carbon stock map of study area.

Table 6
Correlation among variables of regression model for five major tree species.

Species name	Variables	df (*n*-2)	*t*-statistic	*r*	*R* Square	*P* value
S. robusta	CPA and carbon	60	6.89	0.70	0.49	<0.01
	Height and carbon	60	8.58	0.77	0.60	<0.01
	CPA and height	60	6.56	0.68	0.47	<0.01
S. wallichii	CPA and carbon	23	10.75	0.84	0.70	<0.01
	Height and carbon	23	6.83	0.70	0.49	<0.01
	CPA and height	23	5.51	0.62	0.38	<0.01
L. parviflora	CPA and carbon		5.46	0.62	0.38	<0.01
	Height and carbon	29	7.97	0.75	0.56	<0.01
	CPA and height	29	5.70	0.63	0.40	<0.01
T. tomentosa	CPA and carbon	16	9.16	0.79	0.63	<0.01
	Height and carbon	16	11.90	0.86	0.74	<0.01
	CPA and height	16	6.47	0.68	0.46	<0.01
Others	CPA and carbon	49	6.64	0.69	0.47	<0.01
	Height and carbon	49	7.33	0.72	0.52	<0.01
	CPA and height	49	4.66	0.55	0.31	<0.01

from 500–1500 kg/tree (Fig. 6). A total of 188,485 Mg C carbon was estimated in the study site covering an area of 871 ha or on average 216.38 MgC/ha.

Statistical analysis and model validation

Pearson's product-moment correlation coefficient was calculated to analyse the strength of the linear relationship between variables, CPA, LiDAR-derived tree height (referred to as 'height' in the Table) and carbon stock of trees. Relationships among these three variables were calculated for each of the five major species found in the area (Table 6 and Table 7).

There is strong positive correlation (>0.70) between LiDAR-derived tree height and carbon for all five species and the correlation is highly significant ($P < 0.01$). The correlation coefficient between automatic segmented CPA and carbon is more than 0.70, particularly for tree species *S. wallichii* and *T. tomentosa*. On average, correlation coefficients of CPA and carbon, height and carbon, and CPA and height were found to be 0.73, 0.76 and 0.63, respectively. There is, in fact, a significant relationship between CPA, height and carbon stock in the study area, at 95% level of confidence.

Multiple regression models were validated using a randomly selected 30% of independent datasets (total 77) for each tree level species described. For all species, R^2 values were greater than 75%, which means that carbon stock of individual trees estimated using the regression model was able to account for up to 75% of carbon stock measured from the field. Model error varied from 22.48–289.68 kg/tree, depending on tree species, calculated mean carbon stock with 24.85–49.75% of RMSE (Fig. 7).

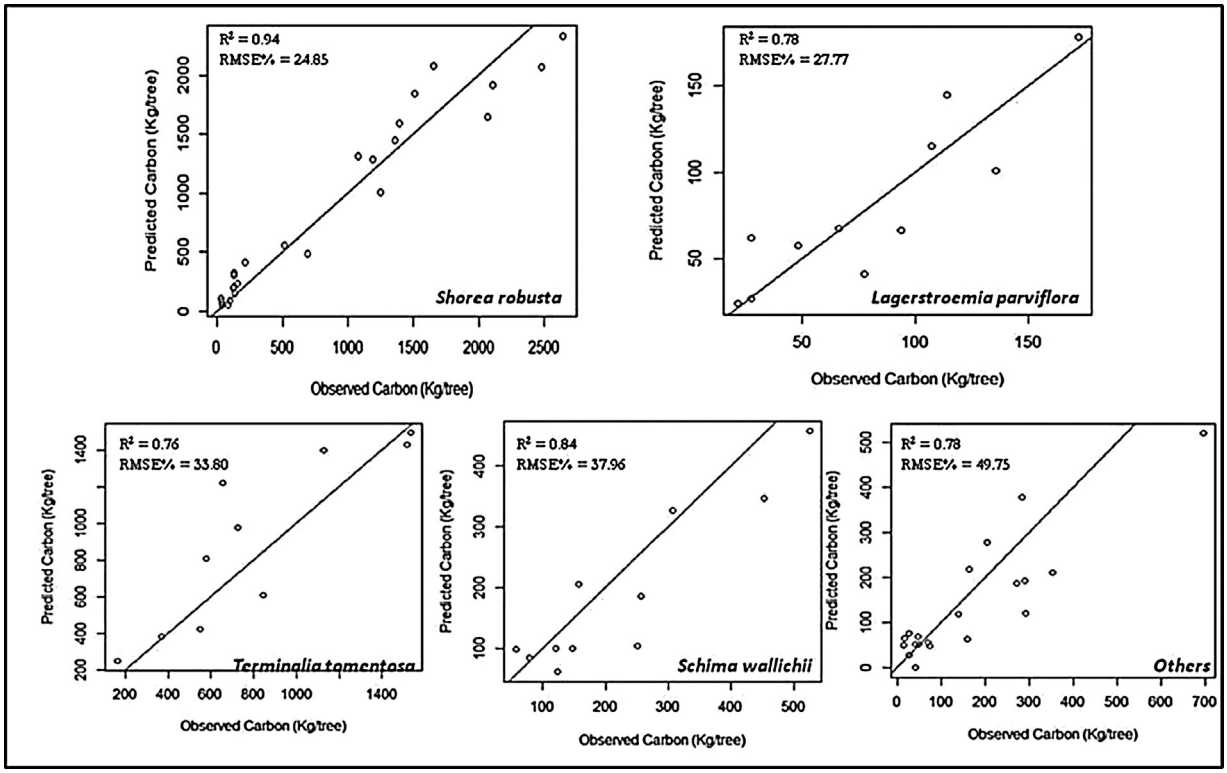

Fig. 7. Scatter plot of observed and predicted carbon stock.

Table 7
Regression coefficients and summary statistics for carbon stocks estimation of five tree species.

Species	β_0	β_1	β_2	*R* square	Adjusted *R* square	Standard error	Observations
S. robusta	−0.877	0.597	1.873	0.66	0.65	0.90	62
S. wallichii	−0.144	1.124	0.883	0.75	0.73	0.61	25
L. parviflora	0.205	0.370	1.494	0.60	0.57	0.58	31
T. tomentosa	−0.126	0.458	1.848	0.82	0.80	0.37	18
Others	0.044	0.616	1.396	0.64	0.63	0.57	51

Discussion

The study area is a natural broadleaved forest with several age gradation and a rich diversity in species composition. CHM generation and its accuracy assessment showed that 54% of field-measured tree height was overestimated and 46% was underestimated by LiDAR height. The coefficient of determination (R^2) of estimated tree height was achieved at 0.76, with RMSE of 3.84 m. Different types of error can be attributed to interpolation of the point cloud data into a grid-based canopy height model, precision of laser height measuring instruments (TruPulse 360 B), random errors that may have been wittingly or unwittingly introduced by field personnel during height measurements. Complexity of the landscapes (undulating, rugged, steep slope) and uneven forest age may contribute to propagating error. LiDAR data (0.8 m point density) used for the study is sufficiently beneficial for estimating tree height but not particularly recommended for individual tree level. Kwak et al. (2007) obtained 0.77, 0.80 and 0.70 R^2 for two coniferous and one deciduous species respectively, using 1.8 m point density, whereas Lim et al. (2003) found 0.68 R^2 value for leaf-on hardwood stands of Ontario, Canada. Similarly, Brandtberg et al. (2003) obtained an accuracy of field and LiDAR height within 1.1 m mean standard error and 0.69 coefficient of determination using high sampling density (e.g., 12 points/m^2) in deciduous forests of North America. In another study, Hemery et al. (2005) found mean differences of 0.53 m between ground measurements and LiDAR height for all species, while for deciduous trees the mean difference was 0.37 m with a standard deviation of 1.43 m. Takahashi et al. (2005) observed an overestimation of LiDAR-derived tree height with an average error of 0.90 m in the mountainous (steep slope >38°) area of Sugi plantation in Japan.

The results of this study, obtained from measure of closeness, showed 67% accuracy with 0.33 *D* value, whereas from a 1:1 spatial correspondence 76% accuracy was obtained applying segmentation on WorldView-2 image and airborne LiDAR data. It could be very difficult to test the bias against all the field measured trees, so we applied the relative area of intersection between segmented objects and reference objects as mentioned by Möller et al. (2007) only for the detected trees although the bias correction is needed for carbon stock mapping in large study area. Lamonaca et al. (2008) discovered that multi-resolution segmentation is preferable for segmenting heterogeneous forests and to explore the dimension of forest structural attributes. Holmgren et al. (2008) found an accuracy increase of 8% in tree crown segmentation by integrating data from the laser-based sensor and optical satellite imagery. Wang et al. (2004) obtained 75.6% segmentation accuracy for spruce and fir forests.

For this study, species classification resulted in an overall accuracy of 58% and Kappa 0.47 in classifying six species, overall accuracy of 56% and Kappa 0.43 for five species, overall accuracy of 63% and Kappa 0.48 for five species and overall accuracy of 73% and Kappa 0.62 for three species, by considering the cluster of CFs as a unit. Species classification in this study was comparatively successful because six broadleaved tree species were classified using WorldView-2 imagery and 0.8 m LiDAR point density data. Moreover, NIR1, NIR2 and red-edge were found to substantially improve classification results for dominant tree species, which was also observed from spectral separability analysis of the image. Voss and Sugumaran (2008) obtained an accuracy rate of 57% and 56%, respectively for five classified deciduous and two evergreen tree species from two hyperspectral datasets.

Correlation analysis demonstrated that the strength of linear relationship between height and carbon was strong ($r > 0.70$) and highly significant ($P < 0.01$) for all five species, whereas correlation coefficients of CPA with carbon and CPA with height were found to be less than that of height with carbon. This could easily be due to the variability of sample correlation coefficient, which depends on sample size and data outliers. Regression models developed for this study were significant in terms of species at $P < 0.05$ and showed R^2 value of 0.66 for *S. robusta*, 0.60 for *L. parviflora*, 0.82 for *T. tomentosa*, 0.75 for *S. wallichii, and* 0.64 for others. Hemery et al. (2005) found a close linear relationship ($R^2 > 0.80$) between crown diameter and stem diameter from 20–50 cm DBH for different species of broadleaved trees. The results are in line with the study of Takahashi et al. (2010), who achieved R^2 of 0.73 for the tree canopy area, height and volume of the Japanese Cedar using low density LiDAR data, QuickBird panchromatic imagery and log-transformed linear regression.

The allometric equations used to estimate AGB were also based on log-transformed linear equations so that they fit well with the models developed to predict carbon stock. Thus, carbon stock predicted from such models yield higher accuracy than models developed using only one variable. A log-transformed multiplicative model was preferred to predict carbon stock as indicated by previous studies, which found such models suitable for predicting stand tree volume and biomass of the trees (Holmgren et al., 2003). Watt and Kirschbaum (2011) found a linear relationship of 0.73 R^2 between height and DBH of even-aged coniferous stands when both variables have been log-transformed. Bartelink (1996) demonstrated the relationship between stem dimensions and biomass of needle leaf forest using log-transformed regression equation, which explained 94% of the variation.

GPS error encountered in the field could not be avoided due to dense canopy, steep slope and atmospheric conditions. Co-registration of WorldView-2 and LiDAR data can be improved by using DEM of LiDAR point cloud data, which can eliminate the shift between trees identified on the image Sun elevation angle and viewing angle of the sensor. Also, in mountain region, shadow, clouds and earth curvature are most important factors for true vertical projection area of canopy.

Conclusion

WorldView-2 satellite imagery and airborne LiDAR data offer promising RS sources for estimating and mapping aboveground carbon stock of tropical broadleaved forests in Nepal. Availability of WorldView-2 offers the possibility of generating very high spatial resolution (0.5 m) images, which showed NIR1, NIR2 and red-edge as the best bands for spectral separability of different tree species, compared to other visible bands of the image. This paper also offers a methodology and approach for other data-scarceapproach

for other countries for measuring carbon stock using the latest state-of-the-art technologies for more accurate data gathering to complement the REDD monitoring, reporting and verification process.

Acknowledgements

This publication is a result of collaborative research carried out by ITC, University of Twente, Netherlands and the International Centre for Integrated Mountain Development (ICIMOD) in three watersheds of Nepal under the REDD+ project. We would like to thank Eak Bahadur Rana, Govinda Joshi and Him Lal Shrestha from ICIMOD, Dr Indra Prasad Sapkota, DFO, Chitwan, and REDD networking committee members for providing valuable information and helping us during field data collection. Our special thanks and appreciation goes to the FRA project and Arbounat for providing airborne LiDAR data and Worldview-2 from Digital Globe for this research.

Appendix A. Supplementary data

Supplementary data associated with this article can be found, in the online version, at http://dx.doi.org/10.1016/j.jag.2015.01.011.

References

Ahmed, R., Siqueira, P., Hensley, S., 2013. A study of forest biomass estimates from LiDAR in the northern temperate forests of New England. Remote Sens. Environ. 130, 121–135.
Asner, G., Mascaro, J., Muller-Landau, H., Vieilledent, G., Vaudry, R., Rasamoelina, M., Hall, J., Breugel, M., 2012. A universal airborne LiDAR approach for tropical forest carbon mapping. Oecologia 168, 1147–1160.
Bartelink, H.H., 1996. Allometric relationships on biomass and needle area of Douglas-fir. For. Ecol. Manage. 86, 193–203.
Belgiu, M., Drăguţ, L., 2014. Comparing supervised and unsupervised multiresolution segmentation approaches for extracting buildings from very high resolution imagery. ISPRS J. Photogramm. Remote Sens. 96, 67–75.
Brandtberg, T., Warner, T.A., Landenberger, R.E., McGraw, J.B., 2003. Detection and analysis of individual leaf-off tree crowns in small footprint, high sampling density lidar data from the eastern deciduous forest in North America. Remote Sens. Environ. 85, 290–303.
Breidenbach, J., Næsset, E., Lien, V., Gobakken, T., Solberg, S., 2010. Prediction of species specific forest inventory attributes using a nonparametric semi-individual tree crown approach based on fused airborne laser scanning and multispectral data. Remote Sens. Environ. 114, 911–924.
Chaturvedi, A.N., Khanna, L., 1982. Forest Mensuration. International Book Distributors, Dehra Dun.
Clinton, N., Holt, A., Scarborough, J., Yan, L., Gong, P., 2010. Accuracy assessment measures for object-based image segmentation goodness. Photogramm. Eng. Remote Sens. 76, 289–299.
Drake, J.B., Knox, R.G., Dubayah, R.O., Clark, D.B., Condit, R., Blair, J.B., Hofton, M., 2003. Above-ground biomass estimation in closed canopy Neotropical forests using LiDAR remote sensing: factors affecting the generality of relationships. Global Ecol. Biogeogr. 12, 147–159.
Erikson, M., Olofsson, K., 2005. Comparison of three individual tree crown detection methods. Mach. Vision Appl. 16, 258–265.
Flewelling, J.W., Hill, Rosette, R., Suárez, J.J., 2008. Probability models for individually segmented tree crown images in a sampling context. In: Proceedings of SilviLaser 2008, 8th international conference on LiDAR applications in forest assessment and inventory, 17–19 September, 2008, SilviLaser 2008 Organizing Committee, Heriot-Watt University, Edinburgh, UK, pp. 284–294.
Gautam, B., Tokola, Hamalainen, T., Gunia, J., Peuhkurinen, M., Parviainen, J., Leppanen, H., Kauranne, V., Havia, T., J, Norjamaki, I., 2010. Integration of airborne LiDAR, satellite imagery, and field measurements using a two-phase sampling method for forest biomass estimation in tropical forests. In: International Symposium on Benefiting from Earth Observation, 4–6 October, Kathmandu.
Gibbs, H.K., Brown, S., Niles, J.O., Foley, J.A., 2007. Monitoring and estimating tropical forest carbon stocks: making REDD a reality. Environ. Res. Lett. 2, 045023.
Hemery, G.E., Savill, P.S., Pryor, S.N., 2005. Applications of the crown diameter–stem diameter relationship for different species of broadleaved trees. For. Ecol. Manage. 215, 285–294.
Holmgren, J., Nilsson, M., Olsson, H., 2003. Estimation of tree height and stem volume on plots-using airborne laser scanning. For. Sci. 49, 419–428.
Holmgren, J., Persson, Å., Söderman, U., 2008. Species identification of individual trees by combining high resolution LiDAR data with multi-spectral images. Int. J. Remote Sens. 29, 1537–1552.
Huang, H., Gong, P., Cheng, X., Clinton, N., Li, Z., 2009. Improving measurement of forest structural parameters by co-registering of high resolution aerial imagery and low density LiDAR data. Sensors (Basel) 9, 1541–1558.
Husch, B., Beers, T.W., Kershaw, J.A., 2003. Forest Mensuration. Wiley.
Hyde, P., Dubayah, R., Walker, W., Blair, J.B., Hofton, M., Hunsaker, C., 2006. Mapping forest structure for wildlife habitat analysis using multi-sensor (LiDAR, SAR/InSAR, ETM, plus, Quickbird) synergy. Remote Sens. Environ. 102, 63–73.
ICIMOD, 2012. A Monitoring Report on Forest Carbon Stocks Changes in Redd Project Sites (Iudikhola, Kayarkhola and Charnawati. Kathmandu, Nepal.
IPCC, 2006. Guidelines for national greenhouse gas inventories. In: IPCCC National Greenhouse Gas Inventories Programme. Institute for Global Environment Strategies, Kanagawa, Japan.
Jochem, A., Hollaus, Rutzinger, M., Hofle, M.B., 2011. Estimation of aboveground biomass in alpine forests: a semi-empirical approach considering canopy transparency derived from airborne LiDAR data. Sensors (Basel) 11, 278–295.
Joseph, S., Herold, M., Sunderlin, W.D., Verchot, L.V., 2013. REDD+ readiness: early insights on monitoring, reporting and verification systems of project developers. Environ. Res. Lett. 8, 34038.
Katoh, M., Gougeon, F.A., Leckie, D.G., 2009. Application of high-resolution airborne data using individual tree crowns in Japanese conifer plantations. J. For. Res. 14, 10–19.
Ke, Y., Quackenbush, L.J., 2011a. A comparison of three methods for automatic tree crown detection and delineation from high spatial resolution imagery. Int. J. Remote Sens. 32, 3625–3647.
Ke, Y., Quackenbush, L.J., 2011b. A review of methods for automatic individual tree-crown detection and delineation from passive remote sensing. Int. J. Remote Sens. 32, 4725–4747.
Kim, S.R., Kwak, D.A., Lee, W.K., Son, Y., Bae, S.W., Kim, C., Yoo, S., 2010. Estimation of carbon storage based on individual tree detection in Pinus densiflora stands using a fusion of aerial photography and LiDAR data (vol 53, pg 885). Sci. China-Life Sci. 53, 1162.
Koch, B., Heyder, U., Weinacker, H., 2006. Detection of individual tree crowns in airborne lidar data. Photogramm. Eng. Remote Sens. 72, 357–363.
Kronseder, K., Ballhorn, U., Böhm, V., Siegert, F., 2012. Above ground biomass estimation across forest types at different degradation levels in Central Kalimantan using LiDAR data. Int. J. Appl. Earth Obs. Geoinf. 18, 37–48.
Kwak, D.-A., Lee, W.-K., Lee, J.-H., Biging, G.S., Gong, P., 2007. Detection of individual trees and estimation of tree height using LiDAR data. J. For. Res. 12, 425–434.
Lamonaca, A., Corona, P., Barbati, A., 2008. Exploring forest structural complexity by multi-scale segmentation of VHR imagery. Remote Sens. Environ. 112, 2839–2849.
Leckie, D., Gougeon, F., Hill, D., Quinn, R., Armstrong, L., Shreenan, R., 2003. Combined high-density lidar and multispectral imagery for individual tree crown analysis. Can. J. Remote Sens. 29, 633–649.
Lefsky, M.A., Cohen, W.B., Parker, G.G., Harding, D.J., 2002. Lidar remote sensing for ecosystem studies. Bioscience 52, 19–30.
Lim, K., Treitz, P., Baldwin, K., Morrison, I., Green, J., 2003. Lidar remote sensing of biophysical properties of tolerant northern hardwood forests. Can. J. Remote Sens. 29, 658–678.
Lindberg, E., Holmgren, J., Olofsson, K., Olsson, H., Wallerman, J.,2008. Estimation of tree lists from airborne laser scanning data using a combination of analysis on single tree and raster cell level, Proceedings of the SilviLaser 2008 Conference, Edinburgh, UK. Available fromgeography.swan.ac.uk/silvilaser/papers/poster_papers/Lindberg.pdf [accessed 0. 106. 2010].
Lobianco, A., Esposti, R., 2010. The Regional Multi-Agent Simulator (RegMAS): An open-source spatially explicit model to assess the impact of agricultural policies. Comput. Electron. Agric. 72, 14–26.
Lovell, J., Jupp, D.L.B., Culvenor, D., Coops, N., 2003. Using airborne and ground-based ranging lidar to measure canopy structure in Australian forests. Can. J. Remote Sens. 29, 607–622.
Lu, D., 2005. Aboveground biomass estimation using Landsat TM data in the Brazilian Amazon. Int. J. Remote Sens. 26, 2509–2525.
Lu, D.S., 2006. The potential and challenge of remote sensing-based biomass estimation. Int. J. Remote Sens. 27, 1297–1328.
Means, J.E., Acker, S.A., Harding, D.J., Blair, J.B., Lefsky, M.A., Cohen, W.B., Harmon, M.E., McKee, W.A., 1999. Use of large-footprint scanning airborne lidar to estimate forest stand characteristics in the Western Cascades of Oregon. Remote Sens. Environ. 67, 298–308.
Möller, M., Lymburner, L., Volk, M., 2007. The comparison index: A tool for assessing the accuracy of image segmentation. Int. J. Appl. Earth Obs. Geoinf. 9, 311–321.
Padwick, C., Deskevich, M., Pacifici, F., Smallwood, S., 2010. WorldView-2 Pan-Sharpening. ASPRS.
Patenaude, G., Milne, R., Dawson, T.P., 2005. Synthesis of remote sensing approaches for forest carbon estimation: reporting to the Kyoto Protocol. Environ. Sci. Policy 8, 161–178.
Peduzzi, A., Wynne, R.H., Thomas, V.A., Nelson, R.F., Reis, J.J., Sanford, M., 2012. Combined use of airborne LiDAR and DBInSAR data to estimate LAI in temperate mixed forests. Remote Sens. 4, 1758–1780.

Popescu, S.C., Wynne, R.H., Nelson, R.F., 2003. Measuring individual tree crown diameter with lidar and assessing its influence on estimating forest volume and biomass. Can. J. Remote Sens. 29, 564–577.
Pouliot, D., King, D., Bell, F., Pitt, D., 2002. Automated tree crown detection and delineation in high-resolution digital camera imagery of coniferous forest regeneration. Remote Sens. Environ. 82, 322–334.
Pu, R., Landry, S., 2012. A comparative analysis of high spatial resolution IKONOS and WorldView-2 imagery for mapping urban tree species. Remote Sens. Environ. 124, 516–533.
Sharma, E.R., Pukkala, T., 1990. Volume Equations and Biomass Prediction of Forest Trees of Nepal. Forest Survey and Statistics Divison, MOFSC, Kathmandu, Nepal.
Sharma, R.P., 2011. Allometric models for total-tree and component-tree biomass of Alnus nepalensis D. Don in Nepal. Indian Forester 137, 1386–1390.
Song, C., Dickinson, M.B., 2008. Extracting forest canopy structure from spatial information of high resolution optical imagery: tree crown size versus leaf area index. Int. J. Remote Sens. 29, 5605–5622.
Takahashi, T., Awaya, Y., Hirata, Y., Furuya, N., Sakai, T., Sakai, A., 2010. Stand volume estimation by combining low laser-sampling density LiDAR data with QuickBird panchromatic imagery in closed-canopy Japanese cedar (*Cryptomeria japonica*) plantations. Int. J. Remote Sens. 31, 1281–1301.
Takahashi, T., Yamamoto, K., Senda, Y., Tsuzuku, M., 2005. Estimating individual tree heights of sugi (*Cryptomeria japonica* D. Don) plantations in mountainous areas using small-footprint airborne LiDAR. J. For. Res. 10, 135–142.
Thapa, R., Watanabe, Motohka, M., Shiraishi, T., Shimada, T.M., 2014a. Calibration of aboveground forest carbon stock models for major tropical forests in central sumatra using airborne lidar and field measurement data, selected topics in applied earth observations and remote sensing. IEEE J., 1–14.
Thapa, R.B., Itoh, T., Shimada, M., Watanabe, M., Takeshi, M., Shiraishi, T., 2014b. Evaluation of ALOS PALSAR sensitivity for characterizing natural forest cover in wider tropical areas. Remote Sens. Environ., 32–41.
Toan, T.L., Quegan, S., Woodward, I., Lomas, M., Delbart, N., Picard, G., 2004. Relating radar remote sensing of biomass to modelling of forest carbon budgets. Clim. Change 67, 379–402.
Toth, C., Ju, H., Grejner-Brzezinska, D., 2011. Matching between different image domains. Photogramm. Image Anal., 37–47.
Ustin, S.L., 2004. Remote Sensing for Natural Resource Management and Environmental Monitoring. Wiley.
Voss, M., Sugumaran, R., 2008. Seasonal effect on tree species classification in an urban environment using hyperspectral data, LiDAR, and an object-oriented approach. Sensors 8, 3020–3036.
Wang, L., Gong, P., Biging, G.S., 2004. Individual tree-crown delineation and treetop detection high-spatial-resolution aerial imagery. Photogramm. Eng. Remote Sens. 70, 351–357.
Watt, M.S., Kirschbaum, M.U.F., 2011. Moving beyond simple linear allometric relationships between tree height and diameter. Ecol. Modell. 222, 3910–3916.
Huang, W., Sun, G., Dubayah, R., Cook, B., Montesano, P., Ni, W., Zhang, Z., 2013. Mapping biomass change after forest disturbance: applying LiDAR footprint-derived models at key map scales. Remote Sens. Environ., 319–332.
Wulder, M.A., Seemann, D., 2003. Forest inventory height update through the integration of lidar data with segmented Landsat imagery. Can. J. Remote Sens. 29, 536–543.
Yamamoto, K., Takahashi, T., Miyachi, Y., Kondo, N., Morita, S., Nakao, M., Shibayama, T., Takaichi, Y., Tsuzuku, M., Murate, N., 2010. Estimation of mean tree height using small-footprint airborne LiDAR without a digital terrain model. J. For. Res. 16, 425–431.
Yaroshenko, A.Y., Potapov, P.V., Turubanova, S.A., 2001. The Last Intact Forest Landscapes of Northern European Russia. Greenpeace Russia and Global Forest Watch, Moscow.